


Competition between weak and α -decay modes in superheavy nuclei

P. Sarriguren ^{*}

Instituto de Estructura de la Materia, IEM-CSIC, Serrano 123, E-28006 Madrid, Spain



(Received 18 October 2021; accepted 10 January 2022; published 18 January 2022)

The competition between α - and β^+ /EC-decay modes is studied systematically in nuclei along the α -decay chains following the synthesis of superheavy nuclei with $Z = 119$ and $Z = 120$. A microscopic approach based on deformed self-consistent Hartree-Fock mean-field calculations with Skyrme forces and pairing correlations is used to describe the β^+ and electron capture weak decays, whereas the α decay is estimated from existing phenomenological expressions. It is shown that α decay is in most cases the dominant decay mode, but interesting instances are identified where the half-lives are comparable, opening the possibility of new pathways towards more neutron-rich nuclei in this region.

DOI: [10.1103/PhysRevC.105.014312](https://doi.org/10.1103/PhysRevC.105.014312)

I. INTRODUCTION

The study of superheavy nuclei (SHN), both theoretically and experimentally, has been one of the most active research topics in nuclear physics during the last decades. Comprehensive overviews of the experimental methods used to synthesize SHN and theoretical approaches employed to their understanding can be found in Refs. [1–8].

Despite the large number of SHN already synthesized with different types of cold and hot fusion reactions, there is a limitation in these reactions that produce neutron-deficient isotopes, far away from the predicted location of the most stable SHN, which is unreachable by fusion reactions with stable beams. Predictions of shell closures from macroscopic-microscopic models based on deformed liquid drop models with shell corrections [9–12] agree with predictions from self-consistent nonrelativistic [13–15] and relativistic [16,17] mean-field models with effective nuclear interactions that produce shell closures at $(Z, N) = (114, 184)$, $(120, 172)$, and $(126, 184)$, depending on the effective interaction used. The sensitivity of the shell closures to the properties of the underlying nuclear forces makes it possible to use SHN as a laboratory to investigate the nuclear force.

Because of the above mentioned experimental difficulties to reach these regions of the nuclear chart, alternative methods are being explored to synthesize more neutron-rich SHN. These methods include fusion reactions with radioactive ion beams and multinucleon transfer reactions [8,18], as well as fusion-evaporation reactions where charged particles are emitted from the compound nucleus [19–22].

Knowledge of the decay properties of SHN is of paramount importance for their identification and for understanding their nuclear structure. The planning, execution, and analysis of experiments leading to SHN production requires a detailed knowledge of the decay modes and half-lives of nuclei in

a very wide range of neutron and proton numbers. Nuclei synthesized in such fusion reactions are basically identified by studying their decay modes, which essentially are dominated by α decay and spontaneous fission (SF). Nevertheless, the study of weak decays is also important, not only to fully characterize all the possible decay modes, but also as a pathway through the predicted island of stability. Weak decays, including electron captures (EC), are not usually considered, partly due to the experimental difficulty to investigate them at the low production rates achieved in present experiments. However, new experimental techniques involving measurements of delayed coincidences between x-rays from the EC process and SF or α decay of the daughter nucleus have been applied to the cases of ^{257}Rf [23], ^{258}Db [24], and ^{244}Md [25] and their EC decays have been determined.

Theoretically, β^+ /EC decays are also more difficult to study. The nuclear structures of parent and daughter nuclei are involved in the process and thus require a microscopic approach to evaluate the nuclear matrix elements connecting the initial with all the final states reached in the process. Present theoretical predictions of weak-decay half-lives in SHN are based on different approaches. Purely phenomenological parametrizations have been used [26] to extrapolate the half-lives to SHN regions, where they are unknown. Other type of calculations neglecting nuclear structure effects as well can be found in Refs. [27–29]. Those approaches consider only transitions connecting the ground states of parent and daughter nuclei, whereas their nuclear matrix elements are assumed to be constant with phenomenological values determined globally for all nuclei, thus neglecting any structural effect. However, the values of such matrix elements may change by orders of magnitude in different calculations. Q_{EC} energies are taken from phenomenological mass models. Therefore, the final estimation of the weak-decay half-lives in those models is reduced to the calculation of the phase-space factors. Half-lives for β^+ /EC decay were also calculated within a proton-neutron quasiparticle random-phase approximation (pnQRPA) that starts with

^{*}p.sarriguren@csic.es

a phenomenological folded-Yukawa single-particle Hamiltonian [30], using masses from a droplet model and standard phase factors.

In this work, β^+ /EC-decay half-lives of SHN are studied from a microscopic point of view, following the work already started in Refs. [31–33]. The method is based on the pnQRPA approach where the parent and daughter partners involved in the decay are described microscopically from a deformed self-consistent Hartree-Fock (HF) calculation with Skyrme interactions and pairing correlations in the Bardeen-Cooper-Schrieffer (BCS) approximation (HF+BCS). In addition to the cases of special interest studied in Refs. [31–33], a systematic study of α and β^+ /EC decay in the SHN is carried out in this work. Rather than the study of decays in isotopic chains, the focus here is the competition between decay modes in the α -decay chain members that follow the synthesis of SHN, including nuclei that are already reachable or are potentially accessible with current (or near future) technological capabilities.

The identification of mass regions where α and β^+ /EC decay may compete would guide experimental work aimed at finding those weak decay modes. Driven by this purpose, different α decay chains, characterized by fixed numbers of N - Z , are systematically studied starting with the new elements to be produced at $Z = 119, 120$ and ending at the nuclides with negative Q_{EC} energies, where no further β^+ /EC decay is possible.

The paper is organized as follows. Section II contains a brief summary of the theoretical formalism used to calculate the energy distribution of the Gamow-Teller (GT) strength, as well as the β^+ /EC-decay half-lives. Section III contains the α and β^+ /EC-decay half-lives for the SHN involved in the different α -decay chains considered in this work, discussing the competition between those decay modes. Section IV contains the final remarks and conclusions.

II. THEORETICAL FORMALISM FOR WEAK DECAYS

The theoretical formalism used in this work to obtain the β^+ /EC-decay half-lives follows the lines described in Refs. [31–33] for SHN. More details of the formalism, as well as the various sensitivities of the half-lives to the model ingredients can be found in Refs. [34–37].

The β^+ /EC-decay half-life, $T_{\beta^+/\text{EC}}$, is obtained after summing all the GT strengths $B(\text{GT}, E_{\text{ex}})$ to states with excitation energies E_{ex} in the daughter nucleus lying below the Q_i energy ($i = \beta^+, \text{EC}$). The strength is weighted with phase-space factors $f^i(Z, Q_i - E_{\text{ex}})$,

$$T_i^{-1} = \frac{(g_A/g_V)_{\text{eff}}^2}{D} \sum_{E_{\text{ex}} < Q_i} f^i(Z, Q_i - E_{\text{ex}}) B(\text{GT}, E_{\text{ex}}), \quad (1)$$

with $D = 6143$ s. A quenching factor of 0.77 is used, such that $(g_A/g_V)_{\text{eff}} = 0.77(g_A/g_V)_{\text{free}}$, with $(g_A/g_V)_{\text{free}} = -1.270$. The total half-life for the combined process is given by $T_{\beta^+/\text{EC}}^{-1} = T_{\beta^+}^{-1} + T_{\text{EC}}^{-1}$.

The nuclear structure calculation used to obtain the GT strength distribution starts with a self-consistent calculation of the mean field. This is achieved from an axially deformed

HF calculation with Skyrme interactions and pairing correlations in the BCS approximation using phenomenological gap parameters. The Skyrme force SLy4 [38] is chosen for that purpose due to its capability to account for a wide variety of nuclear properties throughout the nuclear chart. The mean field calculation generates wave functions, single-particle energies, and occupation amplitudes. The formalism used to solve the HF equations was developed in Ref. [39], assuming time reversal and axial symmetry. The eigenstates of an axially deformed harmonic oscillator potential expressed in cylindrical coordinates are used to expand the single-particle wave functions, using 16 major shells. This basis size is large enough to get convergence of the HF energy. It should also be noted that the use of such a basis, which is adjusted for each nucleus and interaction in terms of the oscillator length and axis-ratio parameters, accelerates the convergence of the results as compared with the spherical basis.

In the mean-field approach, the energy of the different shape configurations can be evaluated with constrained calculations, minimizing the HF energy under the constraint of keeping fixed the nuclear quadrupole deformation parameter β_2 . By varying β_2 one obtains deformation-energy curves (DECs), where the various minima correspond to equilibrium nuclear shapes with the absolute minimum being the ground state. Deformation has been shown to be a critical ingredient in understanding the decay properties of β -unstable nuclei [34–37] and this is also expected in SHN. DECs of some representative cases of SHN, namely, ^{252}Fm , ^{266}Sg , ^{290}Fl , ^{294}Lv , and $^{300}120$, were depicted in Refs. [31–33]. Their analysis shows that the ground states appear at prolate deformations around $\beta_2 \approx 0.3$ in most of the SHN studied here. Only the heaviest nuclei with $Z > 116$ or $N > 170$ exhibit absolute energy minima located around the spherical configuration within a flat region between $\beta_2 = -0.1$ and $\beta_2 = 0.1$. In this work I only consider half-lives from the ground state of the parent nuclei. Half-lives corresponding to shape configurations different from the ground state were studied in Refs. [31–33].

The nuclear structure of odd- A nuclei is described within the equal filling approximation (EFA), blocking the state of the unpaired nucleon characterized by a given spin and parity. In EFA half of the odd nucleon is placed in a given orbital, while the other half is placed in its time-reversed partner. The EFA prescription represents a significant numerical advantage because time-reversal invariance is preserved. By comparing EFA results with those from more sophisticated approaches, it has been shown [40] that EFA is very reliable and precise for most practical applications.

In cases where the spin and parity, J^π , of the nucleus is experimentally determined, the natural choice is to select the blocked state according to the experimental assignments, although in many cases they are derived from systematics. As expected, the experimental assignments are found within the calculated states in the neighborhood of the Fermi level in all the cases studied here. When there is no experimental information on J^π , the blocked state is chosen as the state that minimizes the energy. The sensitivity of the half-lives to J^π has been studied in Refs. [31–33], where calculations were performed for several states close to the Fermi energy with opposite parity. This study is especially interesting given that

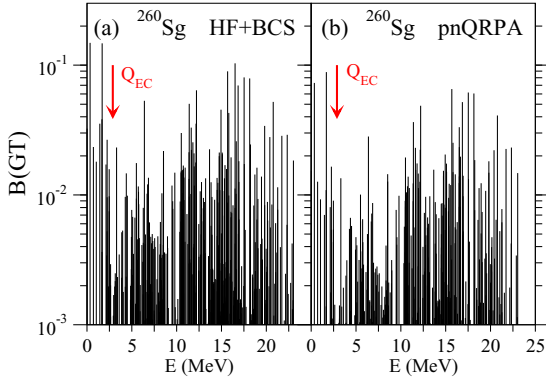


FIG. 1. GT strength distribution of ^{260}Sg calculated within (a) HF+BCS(SLy4) and (b) pnQRPA with spin-isospin separable forces.

small changes in the theoretical description of the nucleus can lead to different J^π values for the ground states, which in turn determine to a large extent the spin and parity of the states reached in the daughter nucleus because of the selection rules of the GT operator.

Once the mean field is constructed, the nuclear matrix elements of the Gamow-Teller operator connecting the ground state of the parent nucleus, which corresponds to the absolute minimum in the DECs, with the excited states of the daughter nucleus are calculated in the pnQRPA [34–37]. The GT strength is calculated on top of the HF+BCS basis with a spin-isospin residual interaction, which is reduced to a separable force. To illustrate the role of this residual interaction, Fig. 1 shows the energy distribution of the GT strength with and without the spin-isospin separable force on the example of ^{260}Sg , which is a representative nucleus in this mass region. The main effect observed is a reduction of the GT strength that increases the β -decay half-life. Although the validity of this approach has still to be justified for SHN, the finite rank separable approximation [41] has been shown to describe properly a large amount of nuclear properties and, in particular, charge-exchange excitations and spin-isospin properties in different mass regions [42].

Other effects on the β -decay properties, such as tensor correlations and the coupling of one- and two-phonon configurations, have been studied in Ref. [43] for Cd isotopes, concluding that typical effects of around 30% are expected in the half-lives, being smaller for heavier isotopes. Similarly, tensor interactions can have an effect on fission barriers and, therefore, on the spontaneous fission half-lives [44], but this would not significantly alter the ratio between α and β decays.

In this work, only allowed GT transitions are considered, whereas first forbidden (FF) transitions are not included. FF transitions are expected to make relevant contributions only in cases where the dominant GT are suppressed and large Q -energy windows provide large phase-space factors. When these conditions are met, although the nuclear matrix elements of FF transitions are orders of magnitude smaller than the GT ones, the phase factors that scale with the fifth power of the energy could make these contributions relevant. However, in the SHN studied here these conditions are not fulfilled

and, therefore, FF contributions are not expected to play a significant role. This can be seen from existing calculations [45], where FF contributions were shown to have little effect on the total β -decay half-lives of SHN.

This model has been used in the past to study GT strength distributions and β -decay half-lives in different regions of the nuclear chart. These studies include medium-mass [46–49] and heavy nuclei [50–52] in the neutron-deficient side, as well as nuclei in the neutron-rich side [53–55], and $f p$ -shell nuclei [56–58]. Spin magnetic dipole excitations, which are the $\Delta T_z = 0$ counterparts of the GT excitations, were also studied within this approach in Refs. [59]. The sensitivity of the GT strength distributions to the nuclear deformation has been used to get information on the nuclear shape by comparing theoretical results with β -decay data [60].

The phase-space factors, f^i , contain two components: positron emission f^{β^+} and electron capture f^{EC} . For a given nucleus, they are computed numerically for each energy value according to Ref. [61],

$$f^{\beta^+}(Z, W_0) = \int_1^{W_0} pW(W_0 - W)^2 \lambda^+(Z, W) dW, \quad (2)$$

where the Fermi function $\lambda^+(Z, W)$ accounts for the Coulomb distortion of the β particle.

The phase factors for electron capture, f^{EC} , are given by

$$f^{\text{EC}} = \frac{\pi}{2} \sum_x q_x^2 g_x^2 B_x, \quad (3)$$

where x stands for the atomic subshell (K, L) from which the electron is captured, q is the energy of the neutrino, g is the radial component of the bound-state electron wave function at the nuclear surface, and B stands for various exchange and overlap corrections [61].

β^+ /EC-decay half-lives depend also on the Q energies. These energies determine the maximum energy available in the process, as well as the values of the phase factors; see Eq. (1). They are given by

$$Q_{\text{EC}} = Q_{\beta^+} + 2m_e = M(A, Z) - M(A, Z - 1) + m_e, \quad (4)$$

written in terms of the nuclear masses $M(A, Z)$ and the electron mass (m_e).

In the cases where the experimental masses are available [63], these values are used to evaluate Eq. (4). But in cases where masses have not been yet measured, theoretical predictions must be used. A large number of mass formulas obtained from different approaches can be found in the literature. They have been discussed for SHN in Refs. [31–33]. In this work I use the masses (WS4+RBF) [62] obtained from a macroscopic-microscopic approach inspired by the Skyrme energy-density functional, including a surface diffuseness correction for unstable nuclei and radial basis function (RBF) corrections. This mass formula has been shown to be very reliable to describe SHN [64].

III. RESULTS

In this Sec. I proceed to compare the half-lives for the α and β^+ /EC decays for nuclei involved in α -decay chains starting at isotopes of $Z = 119$ and $Z = 120$. These α -decay chains

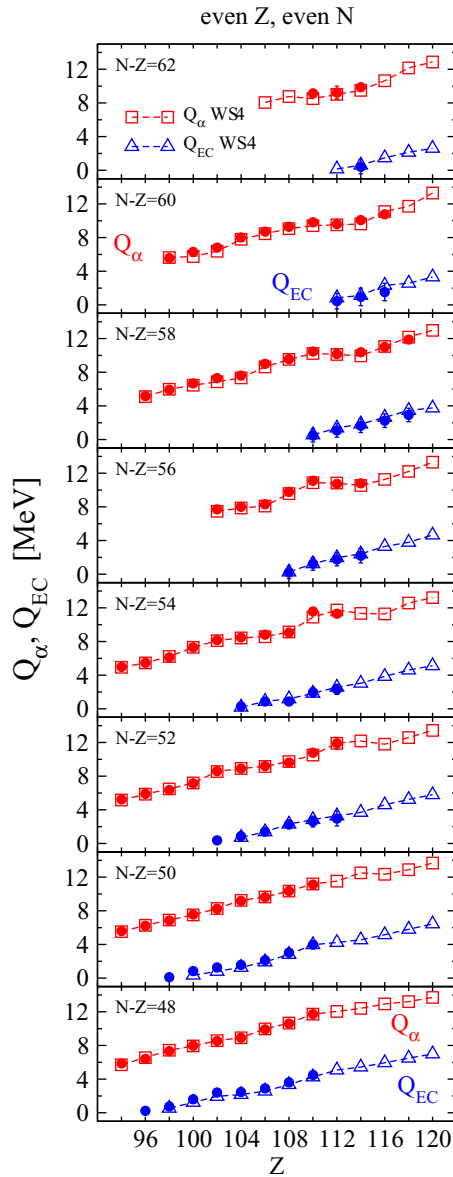


FIG. 2. Q_α (red) and Q_{EC} (blue) energies for even-even nuclei involved in the α -decay chains starting at $Z = 120$ and characterized by different $N-Z$ values from 62 down to 48. Square and triangle open symbols correspond, respectively, to Q_α and Q_{EC} energies calculated with WS4 [62], whereas circles correspond to experimental values [63].

are characterized by a fixed number of the difference $N-Z$. Thus, this value is used to label a given chain.

Comparison between α - and β^+ /EC-decay modes is critical to understand the branching ratios and possible pathways of the original compound nucleus leading to stability. α -decay half-lives are estimated in this work from phenomenological formulas, whereas β^+ /EC-decay half-lives are calculated from the present microscopic calculations. The experimental information of these decay branches in SHN is still very limited. In the cases where experimental information on the total half-life, as well as on the percentage of the corresponding mode intensity are available, the half-lives have been extracted and plotted together with the calculations.

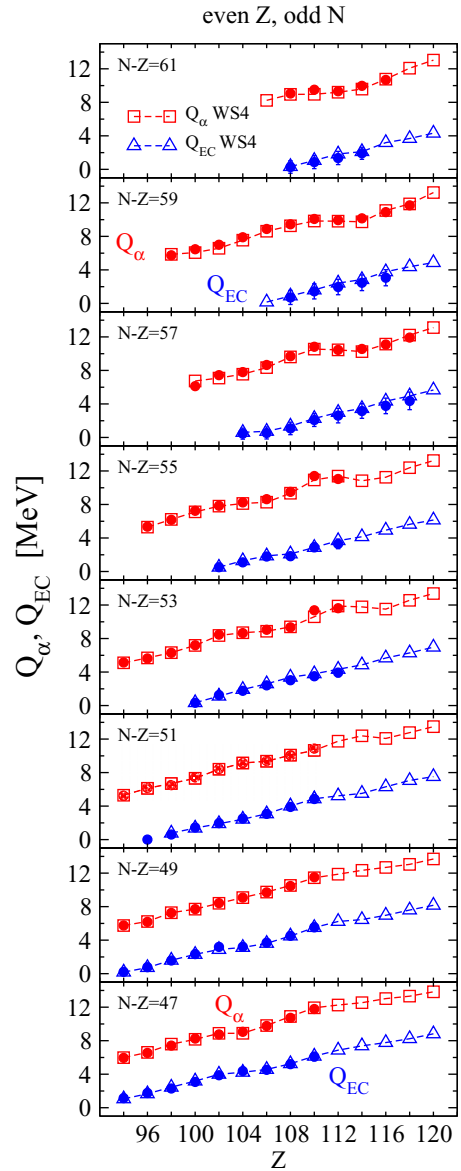
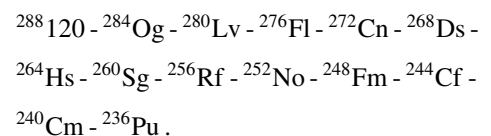


FIG. 3. Same as in Fig. 2, but for α -decay chains with even Z and odd N nuclei.

The half-lives depend on the Q energies which are taken from experiment [63] or from Ref. [62] when the masses are not measured. Figures 2–4 contain Q_α and Q_{EC} energies obtained from experiment [63] and from WS4 [62]. The three figures correspond to the cases of nuclei involved in the α decays with even Z and even N (Fig. 2), with even Z and odd N (Fig. 3), and with odd Z and even N (Fig. 4). Each panel is for a given $N-Z$ value that characterizes the α -decay chains. Only nuclei with $Q > 0$ are considered. As an example, the bottom panel in Fig. 2 with $(N-Z) = 48$ for even values of N and Z corresponds to the following α -decay chain:



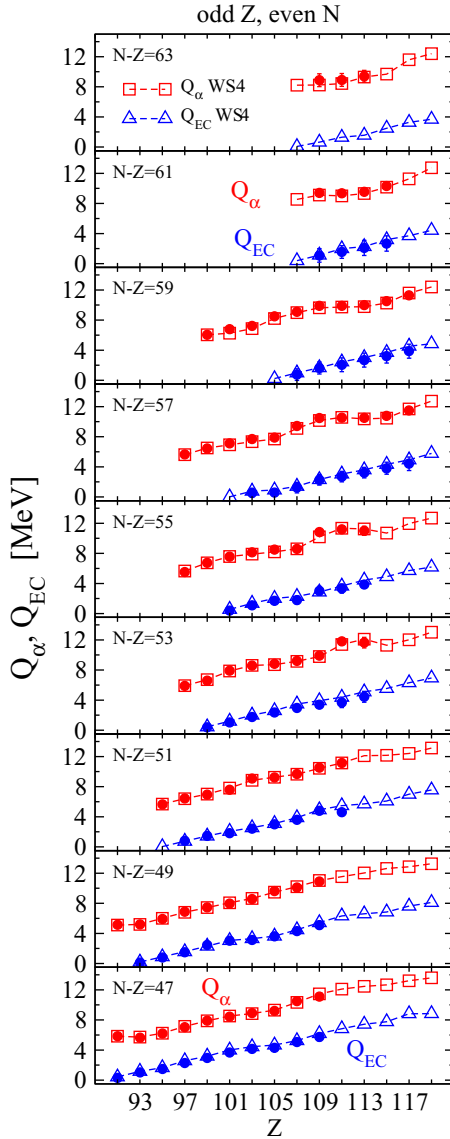
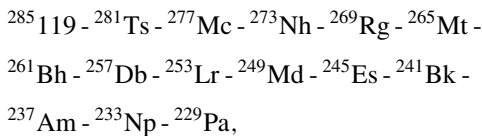


FIG. 4. Same as in Fig. 2, but for α -decay chains with odd Z and even N nuclei involved in the α -decay chains starting at $Z = 119$.

Other panels with different values of $(N-Z)$ correspond to similar α -decay chains, but for different isotopes of a given Z . The α -decay chains in Fig. 3 are similar to Fig. 2, but for odd values of N . Finally, as an example of the α -decay chains involving nuclei with odd Z and even N in Fig. 4, the bottom panel corresponds to the following α -decay chain:



and similarly for the other panels in this figure, but for different isotopes of a given Z .

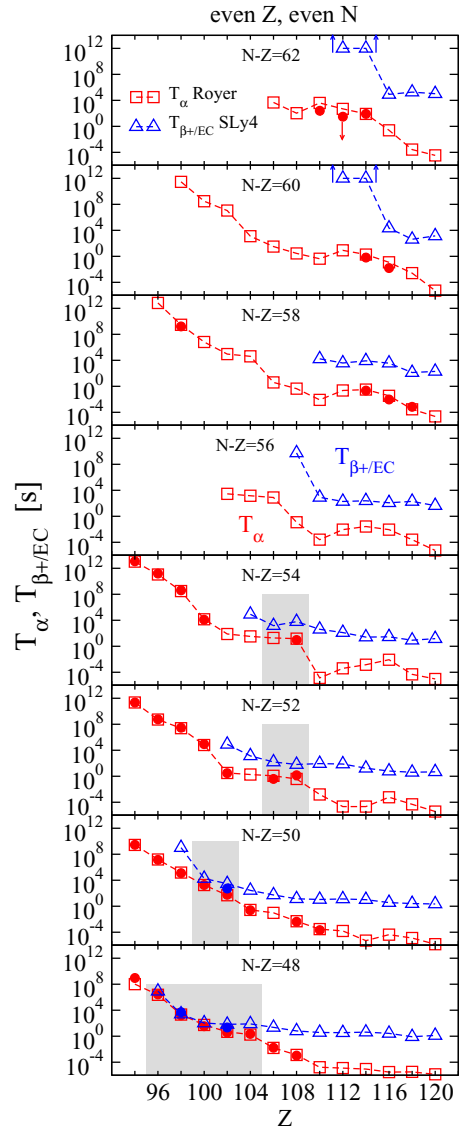


FIG. 5. Calculated half-lives for α (Royer, open squares) and β^+ /EC (SLy4, open triangles) decays. Red and blue points correspond to experimental values [65] for α and β^+ /EC decays, respectively. The gray shaded area highlights the cases where the competition between both decay modes is significant. The set of nuclei considered corresponds to the same α -decay members of Fig. 2.

One can see that the experimental Q values are well reproduced by the mass formula WS4, justifying its use when no experimental information is available. It is worth noting the inflection point in Q_α at around $Z = 110$ in the higher $N-Z$ values, showing a bump which is translated into a relative depression in the corresponding T_α values.

For a given $N-Z$ value in each panel, when Z increases N also increases by the same amount and so do both energies Q_α and Q_{EC} , reflecting general properties of nuclear stability in terms of the relative number of both types of nucleons.

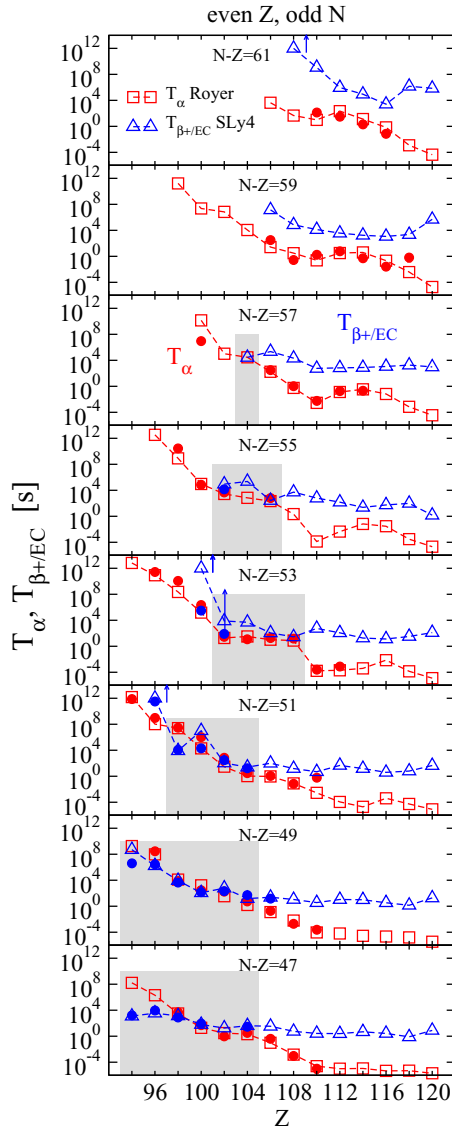


FIG. 6. Same as in Fig. 5, but for the set of nuclei of Fig. 3.

α -decay half-lives have been calculated with a representative phenomenological formula by Royer [66] that produces very reasonable results in the cases studied previously [31–33]. Other formulas available in the literature produce similar results, which do not differ much from the Royer formula for the purpose of this work [31–33].

These values are compared in Figs. 5–7 with the experimentally extracted α -decay half-lives [65], showing a good agreement between them. The figures also contain the experimental and microscopically calculated β^+ /EC-decay half-lives, with good agreement where they have been measured, supporting the reliability of the calculations.

The values of the half-lives $T_{\beta^+/\text{EC}}$ in a given α -decay chain characterized by $N-Z$ exhibit a rather flat behavior in the higher Z nuclei and increase gradually in the lighter partners of the α -decay chain as Q_{EC} decreases in the lighter nuclides of each α -decay chain.

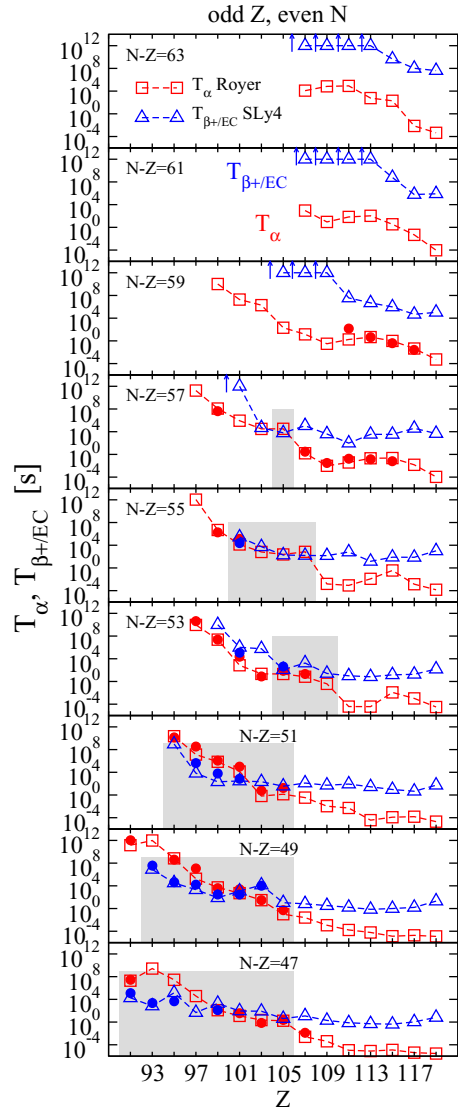


FIG. 7. Same as in Fig. 5, but for the set of nuclei of Fig. 4.

In most cases the decays are dominated by the α mode. This is especially true for nuclei with higher Z ($Z = 110 - 120$). However, one can find regions where the competition between both decay modes is important. In particular, in the α -decay chains with $N-Z$ below 55 and with Z below 108, this competition is relevant. These regions are highlighted with a gray area in the figures for half-lives. Tables I–III contain a more detailed information in these regions, including the spin-parity J^π and the self-consistent quadrupole deformation β_2 of the ground states used in the calculations, the α - and β^+ /EC-decay half-lives, and their ratio $\mathcal{R} = T_{\beta^+/\text{EC}}/T_\alpha$. Only nuclei with ratios \mathcal{R} smaller than 10^3 are included. Similarly to the criterion used to group the different α -decay chains, Table I contains the cases with even numbers of protons and neutrons, Table II is for α -decay chains with even Z and odd N , whereas Table III collects the results for chains with odd Z and even N .

Actually, there are cases where the calculated weak decay is faster than the α decay. This is found specifically in

TABLE I. Spin and parity J^π , quadrupole deformation β_2 , α -decay half-lives T_α , β^+ /EC-decay half-lives $T_{\beta^+/\text{EC}}$, and their ratio \mathcal{R} for members of different α -decay chains with even numbers of protons and neutrons, characterized by $(N-Z)$. Only cases with ratios smaller than 10^3 are considered.

$N-Z$	Nucleus	J^π	β_2	T_α (s)	$T_{\beta^+/\text{EC}}$ (s)	\mathcal{R}
54	^{266}Sg	0^+	0.244	1.90×10^1	1.48×10^3	7.8×10^1
	^{270}Hs	0^+	0.234	1.50×10^1	6.12×10^3	4.1×10^2
52	^{264}Sg	0^+	0.251	1.16×10^0	1.57×10^2	1.4×10^2
	^{268}Hs	0^+	0.239	3.84×10^{-1}	6.44×10^1	1.7×10^2
50	^{250}Fm	0^+	0.276	1.85×10^3	1.87×10^4	1.0×10^1
	^{254}No	0^+	0.284	4.95×10^1	2.89×10^3	5.8×10^1
48	^{240}Cm	0^+	0.269	2.35×10^6	8.50×10^6	3.6×10^0
	^{244}Cf	0^+	0.276	2.16×10^3	2.53×10^3	1.2×10^0
	^{248}Fm	0^+	0.278	5.38×10^1	1.06×10^2	2.0×10^0
	^{252}No	0^+	0.275	4.73×10^0	6.64×10^1	1.4×10^1
	^{256}Rf	0^+	0.271	1.78×10^0	7.91×10^1	4.5×10^1

the cases that follow: ^{247}Cf with $(N-Z) = 51$; ^{237}Pu , ^{241}Cm , ^{245}Cf , and ^{249}Fm with $(N-Z) = 49$; and ^{235}Pu , ^{239}Cm , and ^{243}Cf with $(N-Z) = 47$ in the case of even Z and odd N nuclei. In the case of odd Z and even N nuclei it is found for ^{267}Db with $(N-Z) = 57$, ^{265}Db and ^{269}Bh with $(N-Z) = 55$, for ^{241}Am , ^{245}Bk , ^{249}Es , and ^{253}Md with $(N-Z) = 51$, for ^{235}Np , ^{239}Am , ^{243}Bk , and ^{247}Es with $(N-Z) = 49$, and for ^{229}Pa , ^{233}Np , ^{237}Am , and ^{241}Bk with $(N-Z) = 47$.

TABLE II. Same as in Table I, but for α -decay chains with an even number of protons and an odd number of neutrons.

$N-Z$	Nucleus	J^π	β_2	T_α (s)	$T_{\beta^+/\text{EC}}$ (s)	\mathcal{R}
57	^{265}Rf	$9/2^+$	0.247	2.89×10^4	2.80×10^4	9.7×10^{-1}
55	^{259}No	$9/2^+$	0.259	2.74×10^3	8.92×10^4	3.3×10^1
	^{263}Rf	$3/2^+$	0.251	6.87×10^2	2.30×10^5	3.4×10^2
53	^{267}Sg	$3/2^+$	0.244	2.18×10^2	2.70×10^2	1.2×10^0
	^{257}No	$7/2^+$	0.277	1.90×10^1	7.87×10^3	4.1×10^2
	^{261}Rf	$3/2^+$	0.257	3.21×10^1	4.97×10^3	1.5×10^2
	^{265}Sg	$9/2^+$	0.249	1.02×10^1	1.14×10^2	1.1×10^1
51	^{269}Hs	$9/2^+$	0.240	7.60×10^0	2.81×10^1	3.7×10^0
	^{247}Cf	$7/2^+$	0.276	2.50×10^7	8.49×10^3	3.4×10^{-4}
	^{251}Fm	$9/2^-$	0.285	1.93×10^4	1.01×10^7	5.2×10^2
	^{255}No	$7/2^+$	0.285	2.97×10^1	1.10×10^2	3.7×10^0
49	^{259}Rf	$7/2^+$	0.264	1.06×10^0	2.52×10^1	2.4×10^1
	^{237}Pu	$7/2^-$	0.261	1.82×10^9	5.10×10^8	2.8×10^{-1}
	^{241}Cm	$1/2^+$	0.269	9.57×10^7	1.70×10^6	1.8×10^{-2}
	^{245}Cf	$1/2^+$	0.274	1.25×10^4	8.94×10^3	7.2×10^{-1}
47	^{249}Fm	$7/2^+$	0.277	1.66×10^3	1.16×10^2	7.0×10^{-2}
	^{253}No	$9/2^-$	0.285	3.53×10^1	6.21×10^2	1.8×10^1
	^{257}Rf	$1/2^+$	0.270	1.58×10^0	1.50×10^1	9.5×10^0
	^{235}Pu	$5/2^+$	0.253	1.62×10^8	1.23×10^3	7.6×10^{-6}
	^{239}Cm	$1/2^+$	0.267	2.02×10^6	3.53×10^3	1.7×10^{-3}
	^{243}Cf	$1/2^+$	0.273	3.10×10^3	1.34×10^3	4.3×10^{-1}
	^{247}Fm	$7/2^+$	0.285	1.98×10^1	6.36×10^1	3.2×10^0
	^{251}No	$7/2^+$	0.276	3.03×10^0	1.81×10^1	6.0×10^0
	^{255}Rf	$9/2^-$	0.272	2.07×10^0	4.12×10^1	2.0×10^1

TABLE III. Same as in Table I, but for α -decay chains with an odd number of protons and an even number of neutrons.

$N-Z$	Nucleus	J^π	β_2	T_α (s)	$T_{\beta^+/\text{EC}}$ (s)	\mathcal{R}
57	^{263}Lr	$7/2^+$	0.245	3.10×10^4	5.03×10^4	1.6×10^0
	^{267}Db	$9/2^+$	0.239	3.20×10^4	6.20×10^3	1.9×10^{-1}
55	^{257}Md	$7/2^+$	0.278	1.37×10^4	2.74×10^5	2.0×10^1
	^{261}Lr	$7/2^+$	0.253	6.52×10^2	5.41×10^3	8.3×10^0
	^{265}Db	$9/2^+$	0.245	2.39×10^2	1.92×10^2	8.0×10^{-1}
	^{269}Bh	$9/2^+$	0.236	6.94×10^2	1.58×10^2	2.3×10^{-1}
53	^{263}Db	$9/2^+$	0.252	2.08×10^1	1.22×10^2	5.9×10^0
	^{267}Bh	$5/2^-$	0.242	6.85×10^0	1.76×10^3	2.6×10^2
	^{271}Mt	$9/2^+$	0.227	3.87×10^{-1}	2.63×10^1	6.8×10^1
51	^{241}Am	$5/2^+$	0.265	2.31×10^{10}	9.50×10^8	4.1×10^{-2}
	^{245}Bk	$5/2^+$	0.270	1.33×10^7	6.95×10^3	5.2×10^{-4}
	^{249}Es	$7/2^+$	0.272	7.12×10^5	2.10×10^2	2.9×10^{-4}
	^{253}Md	$7/2^+$	0.281	1.38×10^4	2.97×10^2	2.2×10^{-2}
49	^{257}Lr	$7/2^+$	0.266	6.64×10^{-1}	2.17×10^2	3.2×10^2
	^{261}Db	$9/2^+$	0.260	1.36×10^0	3.61×10^1	2.7×10^1
	^{235}Np	$3/2^+$	0.247	9.66×10^{11}	7.90×10^6	8.2×10^{-6}
	^{239}Am	$5/2^+$	0.260	6.85×10^8	3.23×10^4	4.7×10^{-5}
	^{243}Bk	$5/2^+$	0.268	1.78×10^5	2.07×10^3	1.2×10^{-2}
	^{247}Es	$7/2^+$	0.273	5.32×10^3	7.78×10^1	1.5×10^{-2}
	^{251}Md	$7/2^-$	0.271	5.13×10^2	1.18×10^3	2.3×10^0
	^{255}Lr	$7/2^-$	0.279	3.02×10^1	1.37×10^4	4.5×10^2
	^{259}Db	$9/2^+$	0.265	1.00×10^{-1}	1.07×10^1	1.1×10^2
	^{229}Pa	$5/2^+$	0.211	1.94×10^7	1.87×10^4	1.0×10^{-3}
	^{233}Np	$5/2^+$	0.236	2.67×10^9	6.73×10^2	2.5×10^{-7}
	^{237}Am	$5/2^-$	0.252	2.79×10^7	1.45×10^5	5.2×10^{-3}
47	^{241}Bk	$7/2^+$	0.264	3.78×10^4	4.78×10^1	1.3×10^{-3}
	^{245}Es	$3/2^-$	0.271	1.25×10^2	1.92×10^3	1.5×10^1
	^{249}Md	$7/2^-$	0.271	1.23×10^1	9.11×10^1	7.4×10^0
	^{253}Lr	$7/2^-$	0.272	2.25×10^0	8.05×10^1	3.6×10^1
	^{257}Db	$9/2^+$	0.269	1.73×10^0	4.13×10^0	2.4×10^0

IV. CONCLUSIONS

In this work the weak-decay half-lives of the nuclides involved in the α -decay chains that follow the synthesis of SHN are studied. The method of calculation is based on a self-consistent Skyrme HF+BCS approach. The β^+ /EC-decay half-lives are compared with those of α decay obtained from phenomenological formulas, as well as with the available experimental data.

Although α decay and SF are the dominant decay modes in most of the SHN studied in this work, it is found that weak decays increase progressively their relative importance when one moves towards lower values of the atomic number ($Z < 108$) in a given chain, as well as when one moves towards α -decay chains with lower values of the difference between neutrons and protons ($N-Z < 55$). In fact, the present calculations have identified interesting regions where the β^+ /EC decay is faster than the α decays.

Improved treatments of the residual interaction and inclusion of tensor forces and first forbidden transitions might have an effect on the β -decay half-lives studied here, and it would certainly be worth exploring their impact in the future. However, according to previous studies of these ef-

fects in other mass regions, it could be safely established that the conclusions of this work regarding the competition between α - and β -decay modes will not be significantly altered.

These findings could be used as an experimental guide in searching for weak-decay modes in SHN, pointing to the most favorable cases worth exploring

experimentally, where weak decays could be more easily observed.

ACKNOWLEDGMENT

This work was supported by Ministerio de Ciencia e Innovación MCI/AEI/FEDER,UE (Spain) under Contract No. PGC2018-093636-B-I00.

-
- [1] Special Issue on Superheavy Elements, edited by Ch. E. Düllmann, R.-D. Herzberg, W. Nazarewicz, and Y. Oganessian, *Nucl. Phys. A* **944**, 1 (2015).
- [2] S. Hofmann and G. Münzenberg, *Rev. Mod. Phys.* **72**, 733 (2000).
- [3] Y. Oganessian, *J. Phys. G: Nucl. Part. Phys.* **34**, R165 (2007).
- [4] J. H. Hamilton, D. Hofmann, and Y. T. Oganessian, *Annu. Rev. Nucl. Part. Sci.* **63**, 383 (2013).
- [5] Y. T. Oganessian and V. K. Utyonkov, *Rep. Prog. Phys.* **78**, 036301 (2015).
- [6] S. Hofmann *et al.*, *Eur. Phys. J. A* **52**, 180 (2016).
- [7] S. A. Giuliani, Z. Matheson, W. Nazarewicz, E. Olsen, P. G. Reinhard, J. Sadhukhan, B. Schuettrumpf, N. Schunck, and P. Schwerdtfeger, *Rev. Mod. Phys.* **91**, 011001 (2019).
- [8] G. G. Adamian, N. V. Antonenko, A. Diaz-Torres, and S. Heinz, *Eur. Phys. J. A* **56**, 47 (2020).
- [9] Z. Patyk and A. Sobiczewski, *Nucl. Phys. A* **533**, 132 (1991).
- [10] P. Möller and J. R. Nix, *J. Phys. G: Nucl. Part. Phys.* **20**, 1681 (1994).
- [11] G. G. Adamian, L. A. Malov, N. V. Antonenko, H. Lenske, K. Wang, and S.-G. Zhou, *Eur. Phys. J. A* **54**, 170 (2018).
- [12] G. G. Adamian, N. V. Antonenko, H. Lenske, L. A. Malov, and S.-G. Zhou, *Eur. Phys. J. A* **57**, 89 (2021).
- [13] K. Rutz, M. Bender, T. Bürvenich, T. Schilling, P.-G. Reinhard, J. A. Maruhn, and W. Greiner, *Phys. Rev. C* **56**, 238 (1997).
- [14] A. T. Kruppa, M. Bender, W. Nazarewicz, P.-G. Reinhard, T. Vertse, and S. Ćwiok, *Phys. Rev. C* **61**, 034313 (2000).
- [15] M. Bender, W. Nazarewicz, and P.-G. Reinhard, *Phys. Lett. B* **515**, 42 (2001).
- [16] J. Meng, H. Toki, S. G. Zhou, S. Q. Zhang, W. H. Long, and L. S. Geng, *Prog. Part. Nucl. Phys.* **57**, 470 (2006).
- [17] S. E. Agbemava, A. V. Afanasjev, T. Nakatsukasa, and P. Ring, *Phys. Rev. C* **92**, 054310 (2015).
- [18] V. I. Zagrebaev and W. Greiner, *Phys. Rev. C* **78**, 034610 (2008); **85**, 014608 (2012).
- [19] A. Lopez-Martens *et al.*, *Phys. Lett. B* **795**, 271 (2019).
- [20] F. P. Heßberger, *Eur. Phys. J. A* **55**, 208 (2019).
- [21] J. Hong, G. G. Adamian, and N. V. Antonenko, *Phys. Rev. C* **92**, 014617 (2015); **94**, 044606 (2016); *Phys. Lett. B* **764**, 42 (2017).
- [22] G. G. Adamian, N. V. Antonenko, and W. Scheid, *Phys. Rev. C* **69**, 011601(R) (2004); **69**, 014607 (2004); **69**, 044601 (2004).
- [23] F. P. Heßberger, S. Antalic, A. K. Mistry, D. Ackermann, B. Andel, M. Block, Z. Kalaninova, B. Kindler, I. Kojouharov, M. Laatiaoui, B. Lommel, J. Piot, and M. Vostinar, *Eur. Phys. J. A* **52**, 192 (2016).
- [24] F. P. Heßberger, S. Antalic, D. Ackermann, B. Andel, M. Block, Z. Kalaninova, B. Kindler, I. Kojouharov, M. Laatiaoui, B. Lommel, A. K. Mistry, J. Piot, and M. Vostinar, *Eur. Phys. J. A* **52**, 328 (2016).
- [25] J. Khuyagbaatar, H. M. Albers, M. Block, H. Brand, R. A. Cantemir, A. DiNitto, C. E. Düllmann, M. Gotz, S. Gotz, F. P. Hessberger, E. Jäger, B. Kindler, J. V. Kratz, J. Krier, N. Kurz, B. Lommel, L. Lens, A. Mistry, B. Schausten, J. Uusitalo, and A. Yakushev, *Phys. Rev. Lett.* **125**, 142504 (2020).
- [26] X. Zhang and Z. Ren, *Phys. Rev. C* **73**, 014305 (2006).
- [27] E. O. Fiset and J. R. Nix, *Nucl. Phys. A* **193**, 647 (1972).
- [28] A. V. Karpov, V. I. Zagrebaev, Y. Martinez Palazuela, L. Felipe Ruiz, and W. Greiner, *Int. J. Mod. Phys. E* **21**, 1250013 (2012).
- [29] U. K. Singh, P. K. Sharma, M. Kaushik, S. K. Jain, D. T. Akraway, and G. Saxena, *Nucl. Phys. A* **1004**, 122035 (2020).
- [30] P. Möller, M. R. Mumpower, T. Kawano, and W. D. Myers, *At. Data Nucl. Data Tables* **125**, 1 (2019).
- [31] P. Sarriguren, *Phys. Rev. C* **100**, 014309 (2019).
- [32] P. Sarriguren, *J. Phys. G: Nucl. Part. Phys.* **47**, 125107 (2020).
- [33] P. Sarriguren, *Phys. Lett. B* **815**, 136149 (2021).
- [34] P. Sarriguren, E. Moya de Guerra, A. Escuderos, and A. C. Carrizo, *Nucl. Phys. A* **635**, 55 (1998).
- [35] P. Sarriguren, E. Moya de Guerra, and A. Escuderos, *Nucl. Phys. A* **658**, 13 (1999).
- [36] P. Sarriguren, E. Moya de Guerra, and A. Escuderos, *Nucl. Phys. A* **691**, 631 (2001).
- [37] P. Sarriguren, E. Moya de Guerra, and A. Escuderos, *Phys. Rev. C* **64**, 064306 (2001).
- [38] E. Chabanat, P. Bonche, P. Haensel, J. Meyer, and R. Schaeffer, *Nucl. Phys. A* **635**, 231 (1998).
- [39] D. Vautherin, *Phys. Rev. C* **7**, 296 (1973).
- [40] N. Schunck, J. Dobaczewski, J. McDonnell, J. Moré, W. Nazarewicz, J. Sarich, and M. V. Stoitsov, *Phys. Rev. C* **81**, 024316 (2010).
- [41] N. Van Giai, Ch. Stoyanov, and V. V. Voronov, *Phys. Rev. C* **57**, 1204 (1998).
- [42] A. P. Severyukhin, V. V. Voronov, and N. van Giai, *Prog. Theor. Phys.* **128**, 489 (2012).
- [43] E. O. Sushenok, A. P. Severyukhin, N. N. Arsenyev, and I. N. Borzov, *Phys. At. Nucl.* **82**, 120 (2019).
- [44] S. V. Tolokonnikov, I. N. Borzov, Yu. S. Lyutostansky, and E. E. Saperstein, *JETP Lett.* **107**, 86 (2018).
- [45] T. Marketin, L. Huther, and G. Martinez-Pinedo, *Phys. Rev. C* **93**, 025805 (2016).
- [46] P. Sarriguren, R. Alvarez-Rodríguez, and E. Moya de Guerra, *Eur. Phys. J. A* **24**, 193 (2005).
- [47] P. Sarriguren, *Phys. Rev. C* **79**, 044315 (2009).
- [48] P. Sarriguren, *Phys. Lett. B* **680**, 438 (2009);
- [49] P. Sarriguren, *Phys. Rev. C* **83**, 025801 (2011).
- [50] P. Sarriguren, O. Moreno, R. Alvarez-Rodríguez, and E. M. de Guerra, *Phys. Rev. C* **72**, 054317 (2005).
- [51] O. Moreno, P. Sarriguren, R. Alvarez-Rodríguez, and E. Moya de Guerra, *Phys. Rev. C* **73**, 054302 (2006).
- [52] J. M. Boillos and P. Sarriguren, *Phys. Rev. C* **91**, 034311 (2015).

- [53] P. Sarriguren and J. Pereira, *Phys. Rev. C* **81**, 064314 (2010).
- [54] P. Sarriguren, A. Algora, and J. Pereira, *Phys. Rev. C* **89**, 034311 (2014).
- [55] P. Sarriguren, *Phys. Rev. C* **91**, 044304 (2015).
- [56] P. Sarriguren, E. Moya de Guerra, and R. Alvarez-Rodríguez, *Nucl. Phys. A* **716**, 230 (2003).
- [57] P. Sarriguren, *Phys. Rev. C* **87**, 045801 (2013).
- [58] P. Sarriguren, *Phys. Rev. C* **93**, 054309 (2016).
- [59] P. Sarriguren, E. Moya de Guerra, R. Nojarov, and A. Faessler, *J. Phys. G: Nucl. Part. Phys.* **19**, 291 (1993); **20**, 315 (1994).
- [60] E. Nacher, A. Algora, B. Rubio, J. L. Tain, D. Cano-Ott, S. Courtin, P. Dessagne, F. Marechal, C. Miehé, E. Poirier, M. J. G. Borge, D. Escrig, A. Jungclaus, P. Sarriguren, O. Tengblad, W. Gelletly, L. M. Fraile, and G. Le Scornet, *Phys. Rev. Lett.* **92**, 232501 (2004).
- [61] N. B. Gove and M. J. Martin, *At. Data Nucl. Data Tables* **10**, 205 (1971).
- [62] N. Wang, M. Liu, X. Z. Wu, and J. Meng, *Phys. Lett. B* **734**, 215 (2014).
- [63] M. Wang, W. J. Huang, F. G. Kondev, G. Audi, and S. Naimi, *Chin. Phys. C* **45**, 030003 (2021).
- [64] Y. Z. Wang, S. J. Wang, Z. Y. Hou, and J. Z. Gu, *Phys. Rev. C* **92**, 064301 (2015).
- [65] F. G. Kondev, M. Wang, W. J. Huang, S. Naimi, and G. Audi, *Chin. Phys. C* **45**, 030001 (2021).
- [66] G. Royer, *J. Phys. G: Nucl. Part. Phys.* **26**, 1149 (2000).